The Structural Defects and Optical Performance of Polarization-Maintaining Hollow-Core Photonic Bandgap fiber

Lidong Wang, Meisong Liao, Fei Yu, Liang Chen, Yazhou Wang, Dakun Wu, Tianxing Wang, Lili Hu, and Weiqing Gao

***Abstract*—Hollow core photonic bandgap fiber (HC-PBGF) has potential in the application of fiber optics gyroscopes (FOGs) for its properties of low nonlinearity, and excellent environmental adaptability. However, due to the structural complexity, the HC-PBGF is prone to defects during fabrication process, which will cause degradation of longitude uniformity and optical properties of fiber. The longitudinal non-uniformity of the structure limits the preparation length of HC-PBGF, while high-precision FOGs need to be made with long-distance and high-performance fibers. To facilitate the application of HC-PBGF in high-precision FOG, we studied the instability factors encountered in the fabrication process of polarization-maintaining (PM) HC-PBGF and the induced structural defects, including the fiber core, core-side hole, and fiber diameter defects. According to analyzing the optical performance variation to structural deformation rate, we conducted that the diameter defect has the greatest impact on the fiber properties, while the core-side hole defect has the weakest impact. Based on the fluctuations of optical performance, we revealed the structural deviation tolerance of PM HC-PBGF and provided theoretical reference for fiber fabrication.**

***Index Terms*—Hollow-core photonic bandgap fiber, longitude uniformity, high-precision FOGs, long-distance, structural defects.**

Manuscript received 14 April 2023; revised 15 May 2023; accepted 17 May 2023. Date of publication 24 May 2023; date of current version 2 June 2023. This work was supported in part by the National Natural Science Foundation of China (NSFC) under Grants 51972317 and 61905258, in part by the Key Program for International S&T Cooperation Projects of China under Grant 2018YFE0115600, and in part by the Special Project for Industrialization of High-Tech Science and Technology between Jilin Province and the Chinese Academy of Sciences under Grant 2021SYHZ0029. *(Corresponding author: Meisong Liao.)*

Lidong Wang is with the Key Laboratory of Materials for High Power Laser, Shanghai Institute of Optics and Fine Mechanics, Chinese Academy of Sciences, Shanghai 201800, China, and also with the Center of Materials Science and Optoelectronics Engineering, University of Chinese Academy of Sciences, Beijing 100049, China.

Meisong Liao, Liang Chen, Yazhou Wang, and Tianxing Wang are with the Key Laboratory of Materials for High Power Laser, Shanghai Institute of Optics and Fine Mechanics, Chinese Academy of Sciences, Shanghai 201800, China (e-mail: liaomeisong@siom.ac.cn).

Fei Yu and Lili Hu are with the Key Laboratory of Materials for High Power Laser, Shanghai Institute of Optics and Fine Mechanics, Chinese Academy of Sciences, Shanghai 201800, China, and also with the the Hangzhou Institute for Advanced Study, University of Chinese Academy of Sciences, Hangzhou 310024, China.

Dakun Wu is with the Hangzhou Institute for Advanced Study, University of Chinese Academy of Sciences, Hangzhou 310024, China.

Weiqing Gao is with the School of Electronic Science and Applied Physics, Hefei University of Technology, Hefei 230009, China.

Digital Object Identifier 10.1109/JPHOT.2023.3278930

I. Introduction

With the development of inertial navigation technique, high-performance gyroscopes are widely used in aircraft, missiles, satellite navigation and attitude control [1], [2], [3], [4], [5]. The fiber optic gyroscopes (FOGs) have become the preferred solution for the autonomous navigation due to the advantages of high reliability, large dynamic range, small size, light weight, and easy mass production. The FOGs are moving towards to the direction of high-precision. However, the current panda polarization-maintaining (PM) fiber used in FOGs exhibit deleterious effects, including the Kerr effect [6], Faraday effect [7], and Shupe effects [8], [9]. The noises generated by these effects will degrade the performance of FOGs and limit its high-precision development. Researchers continue to explore ways to improve the performance of FOGs. Among these, hollow core photonic bandgap fibers (HC-PBGF) have aroused great interest. In HC-PBGF, signal propagates in air-core, which shows the superior properties compared with that propagates in panda PM fiber. An important property of HC-PBGF is the extremely low thermal sensitivity [10], which can be further reduced by fiber design [11]. The low thermal sensitivity of HC-PBGF shows potential to improve temperature stability of FOGs. Experiments proves that the Shupe effect of FOGs with HC-PBGF are 3–7 times lower than Panda PM fiber [12], [13]. In addition, HC-PBGF also show the dramatically low nonlinearity effect and magnetic sensitivity [14]. Such a combination of advantages of HC-PBGF makes it an exciting ideal candidate for FOGs.

According to Sagnac effect [15], the long fiber loop is beneficial for improving the precision of FOGs, which requires optical fibers to have both long distance and high performance. However, due to the structural complexity, HC-PBGF is affected by the instability factors during its long-distance fabrication process and prone to structural defects [16]. Previous study shows that the structural defects of HC-PBGF leads to the degradation of fiber longitude uniformity and fiber loss [17], [18], [19]. The problem of long-distance fabrication of HC-PBGF restricts its application to high-precision FOG, and therefore, reducing the structural defects of is a key issue.

In this work, according to structural design, a polarization-maintaining hollow-core photonic bandgap fiber (PM HC-PBGF) with low loss and thermal sensitivity was studied to meet

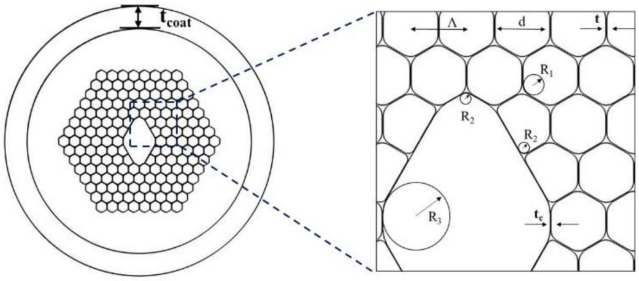

Fig. 1. Transverse geometry of PM HC-PBGF.

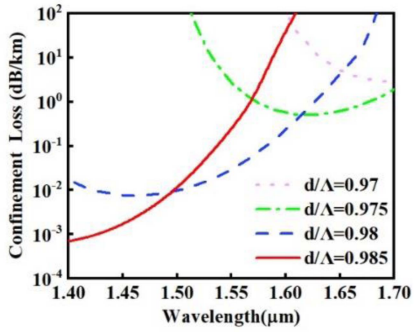

Fig. 2. Confinement Loss (CL) curves of fibers with diverse d/Λ.

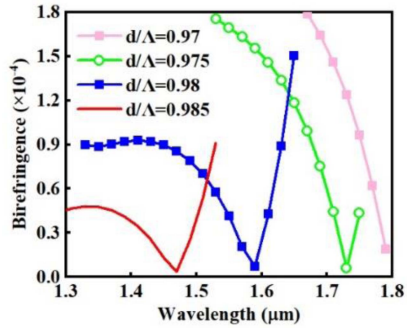

Fig. 3. Birefringence curves of PM HC-PBGF with diverse d/Λ.

the application of FOG. Based on the long-distance requirement, we systematically investigated the instability factors and structural defects of PM HC-PBGF that emerged during the fabrication process, including fiber core defects, core-side hole defects and fiber diameter defects. By analyzing the optical performance drift as a function of structural deformation rate, we revealed the geometrical deviation tolerance of PM HC-PBGF. This work provides theoretical argument for influence of structural defects on optical properties and reference for fiber fabrication.

II. The Structure and Fundamental Properties of HC-PBGF

A. Fiber Structure

For the application of FOG, a kind of polarization-maintaining fiber is studied here, and the fiber has a 9-cell rhombic core, which was studied in our previous work [20], shown in Fig.1. The birefringence is originated from the core diameter asymmetry along the two orthogonal axes. The rhombic core fiber was firstly fabricated into 4-cell fiber by removing 4 capillaries in the center of preform [21]. If the 9 capillaries are removed from preform, the fiber will be enlarged to make the 9-cell fiber. The fiber discussed here has a comparable large-core which is beneficial for reducing its loss [22]. Several parameters are used to describe the fiber structures. Cladding is composed of periodic rounded hexagons [23] with an air pore diameter d and the lattice spacing $\Lambda = 4.49\ \mu$m; the pore fillet radius of the cladding and first cladding ring are $R_1 = 0.23\Lambda$ and $R_2 = 0.11\Lambda$, respectively. The core wall thickness is half the cladding wall thickness t, which is beneficial for reducing the normalized interface field intensity and cladding mode power, thereby alleviating surface scattering and reducing fiber loss [22], [24]. The coating thickness is t_{coat}. The optical properties of HC-PBGF are largely related to the cladding air-filling fraction f which is defined as [23]:

$$f = \left(\frac{d}{\Lambda}\right)^2 \left[1 - \left(1 - \frac{\pi}{2\sqrt{3}}\right)\left(\frac{2R_1}{d}\right)\right] \quad (1)$$

The cladding air-filling fraction f is related to Λ, d, and R1. To unify the variables, we fixed Λ and R1, thus, f is only related to d. To study the fiber optical performance variation trend to fiber structure, f, d/Λ is evaluated at 0.97, 0.975, 0.98 and 0.985.

B. Fundamental Properties

1) Confinement Loss: The finite element calculation method was applied to calculate the effective refractive index n_{eff} incorporating the perfect matching layer boundary conditions. The confinement loss (CL) was obtained by a secondary calculation via the imaginary part of n_{eff} of the fundamental mode [25]. The CL is the basic indicator for evaluating the rationality of structural design, which is an important optical property, therefore, we only consider the CL here. The fiber attenuation of the fundamental mode (FM) as a function of the geometry parameter d/Λ was shown in Fig. 2. Blue shift of the center wavelength occurred as d/Λ expands, which was consistent with the literature [23]. The fiber had a minimum CL of 0.029 dB/km in 1550 nm when the $d/\Lambda = 0.98$.

2) Birefringence: The difference between the real parts of n_{eff} of the two polarized FMs indicates birefringence, which can be calculated using following equation.

$$B = |\mathrm{Re}(n_{effx} - n_{effy})| \quad (2)$$

Fig. 3 showed the birefringence curves of the fibers. It could be inferred that there was a trade-off between the CL and birefringence, because the two parameters exhibited a negative correlation. Although the birefringence of fiber with $d/\Lambda = 0.98$ was only 4.15×10^{-5} at 1550 nm, the PM property was still obvious. There was a practical example of HC-PBGF used in FOG, and its birefringence value of HC-PBGF was measured to be 6×10^{-5} [26], which was comparable to that of the fiber here.

This shows that the HC-PBGF with birefringence of $\times 10^{-5}$ can meet the requirement of polarization-maintenance.

In this paper, the thermal coefficient of delay (TCD) was employed to describe the fiber thermal sensitivity. Fiber TCD with different structural parameters were obtained using the following equation [11]:

$$TCD = \varepsilon_{zz}\frac{\partial\beta}{\partial\omega} - \overline{\alpha}\lambda D + \frac{\partial}{\partial\omega}\left(\frac{\overline{\Delta n}}{\Delta T}\frac{k_0^2}{\beta}n_{glass}\eta\left(\lambda\right)\right) \quad (3)$$

where ω was angular velocity, n_{glass} was the refractive index of glass, and $\eta(\lambda)$ was the fraction of mode power carried in glass, $\overline{\alpha}$ was the power-weighted average coefficient of expansion, and $\frac{\overline{\Delta n}}{\Delta T}$ was the power-weighted average refractive index change with temperature. ε_{zz} was the elongation strain coefficient obtained by the area-weighted product of Young's modulus and thermal expansion coefficient [12].

Fig. 4(a) showed the TCD curves under different d/Λ values, which shift to shorter wavelengths substantially as d/Λ increased, consistent with the bandgap. Consequently, the TCD value at a fixed wavelength could be tuned by choosing the proper parameter d/Λ. Compared with other geometries, the fiber with d/Λ = 0.98 had TCD values closest to 0 ps/km/K at 1550 nm; therefore, we selected HC-PBGF with this structural parameter as the target for the next step of the analysis. Fiber coating is an organic material with a high thermal expansion coefficient, which attached on the surface of bare fiber. The predominant thermal response of coating to fibers is apparent elongation [12], which improves the TCD value. Fig. 4(b) showed the TCD curves of the fibers with a series of coating thicknesses when d/Λ = 0.98 (coating thickness was represented by coating diameter Dcoat). As expected, the large thermal expansion rate of the coating results in the longitudinal elongation of the fiber, thereby causing additional thermal delay. As observed in the calculation results, the PM HC-PBGF achieved an ultra-low TCD value of 0.0016 ps/km/K at 1550 nm when Dcoat = 113.6 μm.

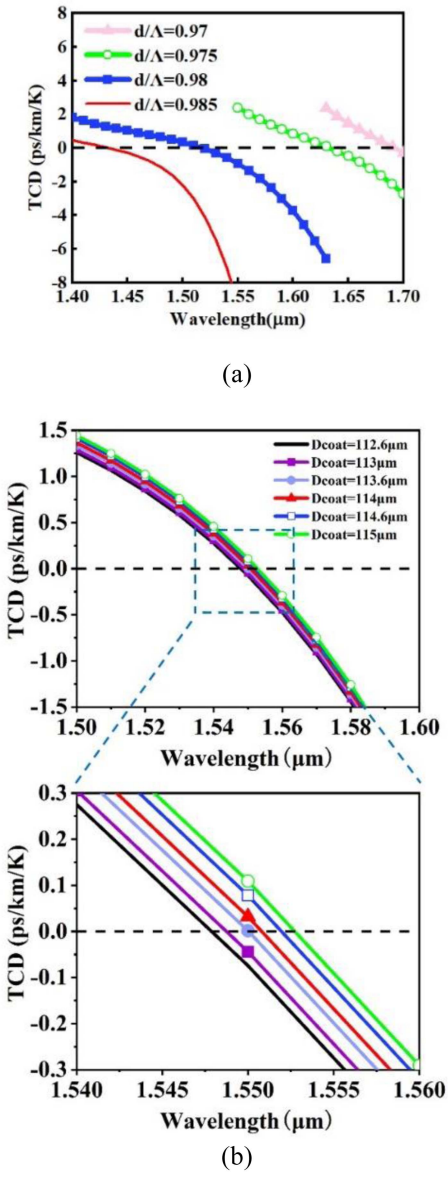

Fig. 4. (a) TCD curves of PM-HC-PBGF with different d/Λ. (b) TCD curve in different coating thickness of PM HC-PBGF.

III. Structural Defects

PM HC-PBGF is fabricated via a two-stage stack-and-draw technique, which includes preform drawing to the cane and cane drawing to the fiber. High-quality PM HC-PBGF requires strict preparation conditions. Any instability will cause longitudinal defects in the fiber. The instabilities include air pressure jitter and non-uniformity of the cane. In this study, the optical fiber structural defects caused by their instabilities and the influence on optical properties were studied, revealing structural deformation tolerance of PM HC-PBGF.

A. Core Defect

In fiber drawing process, different air pressures are applied to the core and cladding to maintain the shape of the air hole. However, the core is larger in size and more prone to deformation than the cladding hole; therefore, the core shape is more susceptible to air pressure fluctuations. The original size of the core is around Dc = 13.3 μm. We studied the core defect according to its deformation from −3%Dc to 3%Dc, and Fig. 5(a) shows a schematic diagram of this case. Fig. 5(b) shows the CL of the deformed fibers. As the core size gradually increased, a slight blue shift of the bandgap occurred, and thus the fluctuation of CL at 1550 nm was small. As the bandgap moved, the birefringence changed significantly, as shown in Fig. 5(c).

The deformed core from −3%Dc to 3%Dc resulted in birefringence change of approximately 1×10^{-4} at 1550 nm. Like birefringence, the TCD curve blue shifted as the core size increased, shown in Fig. 5(d), which resulted in an obvious change of TCD from 0.76 to −1.34 ps/km/K at 1550 nm. Note that the TCD of fiber here was obtained with coating attached, and Dcoat = 113.6 μm.

B. Core-Side Hole Defect

During the cane fabrication process, the cladding hole is prone to defects which evolves more obviously after pre-pared into an

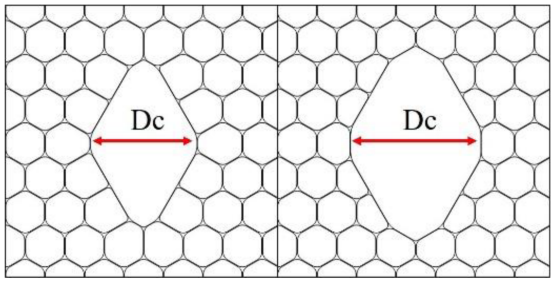

(a)

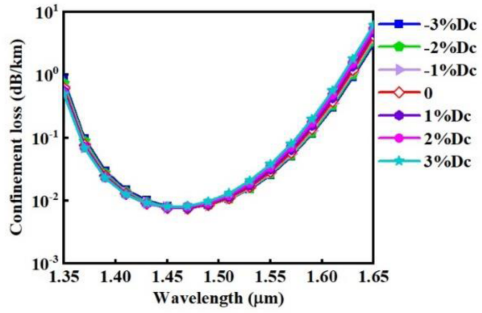

(b)

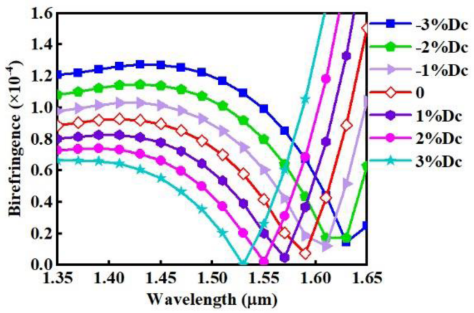

(c)

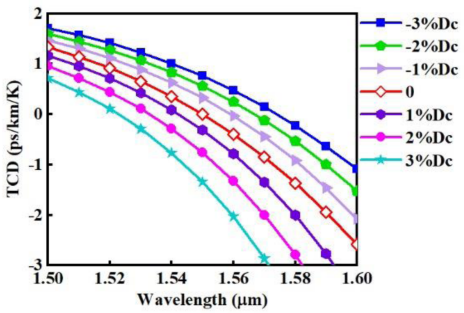

(d)

Fig. 5. (a) Core deformation (b) CL curves of HC-PBGF for different core deformations (c) Birefringence curves for HC-PBGF in different core deformations (d) TCD curves of HC-PBGF for different core deformations.

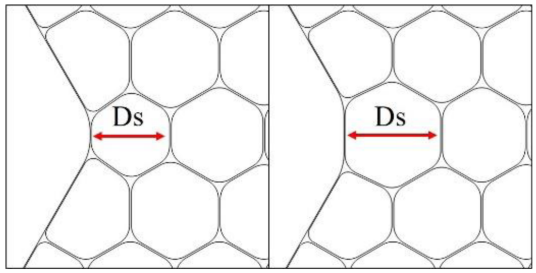

(a)

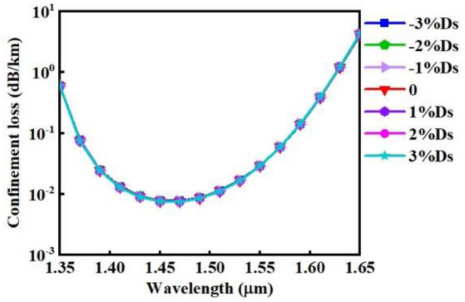

(b)

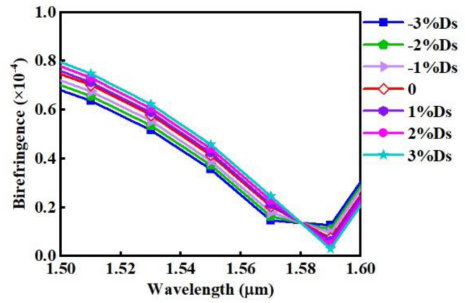

(c)

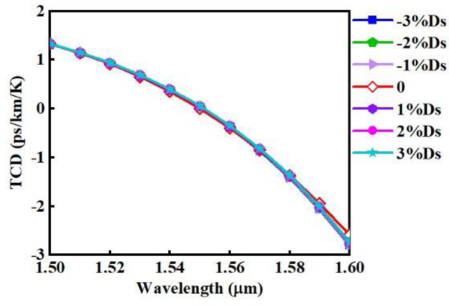

(d)

Fig. 6. (a) Core-side hole deformation (b) CL curves of HC-PBGF with core-side hole deformations (c) Birefringence curves of HC-PBGF with different core-side hole deformations (d) TCD curves of HC-PBGF with different core-side hole deformations.

optical fiber. The first cladding ring layer of the fiber has the greatest impact on signal transmission, so we only discuss the cladding defects caused by it in this study, that is, the deformation of the core-side hole diameter Ds. Fig. 6(a) showed a schematic diagram of this case, and the size deformation of the core-side holes evaluated in this study changed from −3%Ds to 3%Ds. The adjacent structures of the core-side holes, including the core and cladding holes, also underwent corresponding deformations. Fig. 6(b) depicted the CL curves under the deformed core-side hole, and it could be seen that the bandgap was almost unchanged. As the core-side hole deformation changed from

−3%Ds to 3%Ds, the birefringence curve red shifted, as shown in Fig. 6(c). This resulted in an increase in the birefringence of approximately 1×10^{-5} at 1550 nm. Fig. 6(d) showed the TCD of the deformed fibers, and it could be seen that the change in the TCD curve was also very small, similar to the change of the bandgap curve. Note that the TCD of fiber here was obtained with coating attached, and Dcoat = 113.6 μm.

C. Fiber Diameter Defect

Except for the core-side hole defect, the diameter of the cane is also prone to longitudinal non-uniformity, which is amplified in the fiber drawing step. The diameter defect in this study is the diameter deformation from −3%D to 3%D; Fig. 7(a) was a schematic diagram of this case. As the fiber diameter increased, the entire microstructure, including periodic lattice spacing, was proportionally scaled up, so the bandgap curve red shifts significantly. This resulted in the CL of the optical fiber decreased from 0.2 dB/km to 0.01 dB/km at 1550 nm. Similarly, the birefringence and TCD also changed obviously, shown in Fig. 7(c) and (d). The birefringence changed from 5.4×10^{-6} to 7.14×10^{-5} at 1550 nm and the fiber TCD changed from −2.5 ps/km/K to 1.22 ps/km/K as fiber diameter increased from −3%D to 3%D. Therefore, defects in fiber diameter had the greatest influences on optical performance. Note that the TCD of fiber here was obtained with coating attached, and Dcoat varied proportionally with fiber diameter.

Different defects have different effects on optical properties, and we made an analogy of the changes in optical properties caused by these defect types. The deformation rate of the fiber core size Dc, core-side hole size Ds, and fiber diameter D ranged from −3% to 3%, and the wavelength discussed here was selected as 1550 nm.

Fig. 8(a) showed the CL variation of the fiber under different defects. The fiber diameter had the greatest impact on the CL under the same deformation rate, which was one order of magnitude higher than other deformations because of the equal proportional change in the periodic lattice. Fig. 8(b) showed the birefringence change in the fibers under different defects at 1550 nm. The birefringence of the PM HC-PBGF was dependent on the core structure, and thus, the core defect had the most obvious influence on it. In the original HC-PBGF Birefringence-Wavelength curve, shown in Fig. 5(b), there exists a minimum value point near which the propagation constants of the polarization modes X and Y are very close. However, for different waveguide structures, the position of the minimum value point is also different. When the core deformation is 2%, the minimum value point of birefringence is closest to 1550 nm, in which the birefringence of the fiber is the smallest. Under other core deformation rates, the minimum point of birefringence gradually moves away from the 1550 nm, in which birefringence increases. Therefore, there may be a turning point in the Birefringence-Deformation rate curve. This theory is also applicable to the birefringence change curve caused by fiber diameter deformation. When the core deformation rate changed from −3% to 3%, the maximum birefringence change reaches 1×10^{-4}. At the same time, the birefringence also moved with the bandgap curve; therefore, the

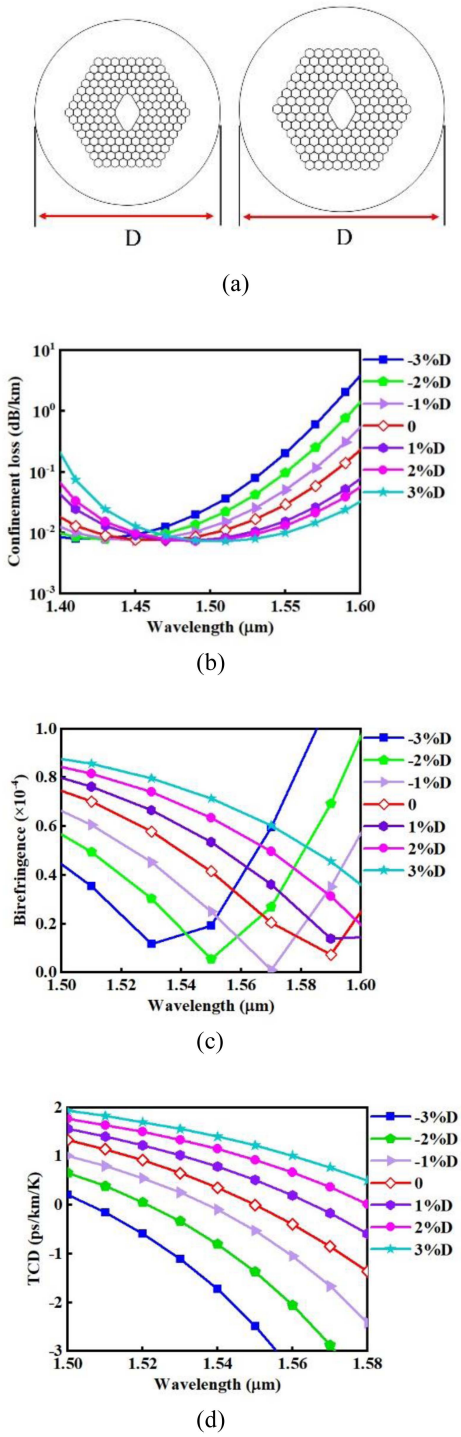

Fig. 7. (a) Diameter deformation. (b) Attenuation curves of HC-PBGF with different diameter deformations. (c) Birefringence curves of HC-PBGF with different diameter deformations. (d) TCD curves of HC-PBGF with different diameter deformations.

fiber diameter defect also affected birefringence. The effect of the core-side hole defect on the birefringence was the smallest, which was about 1×10^{-5}. Fig. 8(c) showed the TCD change in the fiber under different defects. The TCD of the fiber also moved with the bandgap to a large extent, hence, it was most affected by the fiber diameter defect and had the largest change

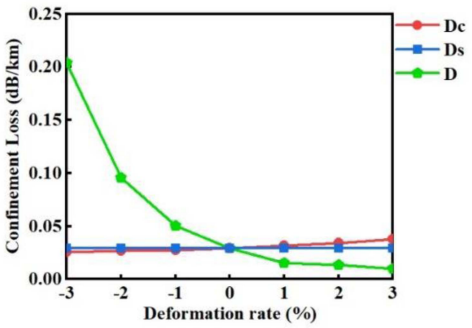

(a)

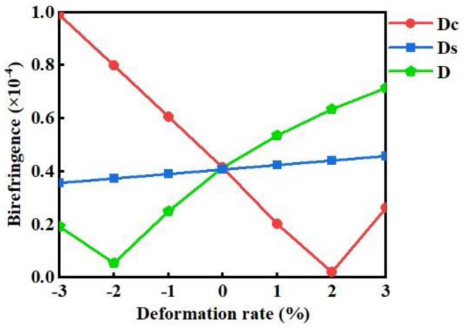

(b)

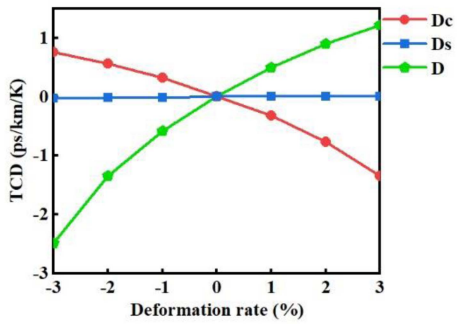

(c)

Fig. 8. (a) Fiber attenuation under different structural deformations at 1550 nm. (b) Fiber birefringence under different structural deformations at 1550 nm. (c) Fiber TCD under different structural deformations at 1550 nm.

TABLE I
OPTICAL FIBER PERFORMANCE UNDER DIFFERENT DEFECTS

	Deformation	CL (dB/km)	Birefringence ($\times 10^{-5}$)	TCD (ps/km/K)
Original structure	0	0.02922	4.15	0.0016
Core defect	-3%Dc	0.026	9.90	0.76
	3%Dc	0.038	2.60	-1.34
Core-side hole defect	-3%Ds	0.0293	3.56	-0.025
	3%Ds	0.0292	4.57	0.007
Fiber diameter defect	-3%D	0.20	1.92	-2.5
	3%D	0.01	7.14	1.22

of 3.72 ps/km/K. In addition, core defects caused changes in the mode propagation constants, leading to fluctuations in the signal delay times, further affecting the TCD. The effect of the core-side hole defect on the TCD was negligible, and was two orders of magnitude smaller than that of the core and fiber diameter defects. Table I showed the CL, birefringence and TCD values of the fibers with different defects and deformations. To maintain the stability of the optical properties of the fiber, the fiber diameter and core structure defects must be as small as possible.

IV. CONCLUSION

In this study, a kind of PM HC-PBGF was studied. By tuning the microstructure, an ultra-low loss fiber was obtained, which had CL and birefringence of 0.029 dB/km and 4.15×10^{-5} at 1550 nm, respectively. For improving temperature stability of FOG, the microstructure and coating of HC-PBGF are further designed to have ultra-low thermal sensitivity, and the TCD is close to 0 ps/km/K. To promote long-distance application of PM HC-PBGF in high-precision FOGs, the instabilities induced fiber structural defects in the fabrication process was investigated, including the core defects, the core-side hole defects and diameter defects. When the deformation rate changed from -3% to 3%, the fiber diameter defect had the greatest impact on the optical performance, with changes in CL, birefringence, and TCD of 0.19 dB/km, 6.59×10^{-5}, and 3.72 ps/km/K, respectively. This is because of the proportional change in the lattice structure and the resulting significant bandgap shift. In addition, the influence of fiber core defect on the birefringence and TCD was also obvious, because the signal propagation constant mainly depends on the core shape. Under the same deformation rate, the core-side hole had the weakest influence on the optical properties, and its resulted fluctuation of optical performance was one or two orders of magnitude smaller than other defects. Therefore, to maintain the stability of the optical performance, the core shape and fiber diameter defects should be kept as small as possible. The study of the defect tolerant characteristics provides theoretical reference for the long-distance fabrication of PM HC-PBGF for high-precision FOGs applications.

DISCLOSURE

The authors declare no conflict of interest.

REFERENCES

[1] H. C. Lefèvre et al., "The fiber optic gyro 'adventure' at Photonetics, iXsea and now iXblue," *Proc. SPIE*, vol. 11405, pp. 10–29, 2020.
[2] G. A. Pavlath, "Fiber optic gyros: The vision realized," in *Proc. Opt. Fiber Sensors*, Cancun, Mexico, 2006, pp. 23–27.
[3] F. Zarinetchi and S. Ezekiel, "Observation of lock-in behavior in a passive resonator gyroscope," *Opt. Lett.*, vol. 11, pp. 401–403, Jun. 1986, doi: 10.1364/OL.11.000401.
[4] J. Jin, T. Zhang, L. Kong, and K. Ma, "In-orbit performance evaluation of a spaceborne high precision fiber optic gyroscope," *Sensors*, vol. 18, no. 1, Dec. 2018, Art. no. 106, doi: 10.3390/s18010106.
[5] M. J. Digonnet and J. N. Chamoun, "Recent developments in laser-driven and hollow-core fiber optic gyroscopes," in *Proc. SPIE*, vol. 9852, 2016, Art. no. 985204.

[6] S. Ezekiel, J. L. Davis, and R. W. Hellwarth, "Observation of intensity induced nonreciprocity in a fiber-optic gyroscope," *Opt. Lett.*, vol. 7, no. 9, pp. 457–459, Sep. 1982, doi: 10.1364/OL.7.000457.

[7] P. Liu, X. Li, X. Guang, G. Li, and L. Guan, "Bias error caused by the Faraday effect in fiber optical gyroscope with double sensitivity," *IEEE Photon. Technol. Lett.*, vol. 29, no. 15, pp. 1273–1276, Aug. 2017, doi: 10.1109/LPT.2017.2723007.

[8] C. Zhang, S. Du, J. Jin, and Z. Zhang, "Thermal analysis of the effects of thermally induced nonreciprocity in fiber optic gyroscope sensing coils," *Optik*, vol. 122, no. 1, pp. 20–23, Jan. 2011, doi: 10.1016/j.ijleo.2009.10.004.

[9] D. M. Shupe, "Thermally induced nonreciprocity in the fiber-optic interferometer," *Appl. Opt.*, vol. 19, no. 5, pp. 654–655, Mar. 1980, doi: 10.1364/AO.19.000654.

[10] R. Slavík et al., "Ultralow thermal sensitivity of phase and propagation delay in hollow core optical fibres," *Sci. Rep.*, vol. 5, Oct. 2015, Art. no. 15447, doi: 10.1038/srep15447.

[11] E. N. Fokoua, M. N. Petrovich, T. Bradley, F. Poletti, D. J. Richardson, and R. Slavík, "How to make the propagation time through an optical fiber fully insensitive to temperature variations," *Optica*, vol. 4, no. 6, pp. 659–668, Jun. 2017, doi: 10.1364/OPTICA.4.000659.

[12] V. Dangui, H. K. Kim, M. J. F. Digonnet, and G. S. Kino, "Phase sensitivity to temperature of the fundamental mode in air-guiding photonic-bandgap fibers," *Opt. Exp.*, vol. 13, no. 18, pp. 6669–6684, Sep. 2005, doi: 10.1364/OPEX.13.006669.

[13] S. Blin, H. K. Kim, M. J. F. Digonnet, and G. S. Kino, "Reduced thermal sensitivity of a fiber-optic gyroscope using an air-core photonic-bandgap fiber," *J. Lightw. Technol.*, vol. 25, no. 3, pp. 861–865, Mar. 2007, doi: 10.1109/JLT.2006.889658.

[14] M. Digonnet, S. Blin, H. K. Kim, V. Dangui, and G. Kino, "Sensitivity and stability of an air-core fibre-optic gyroscope," *Meas. Sci. Technol.*, vol. 18, no. 10, Sep. 2007, Art. no. 3089, doi: 10.1088/0957-0233/18/10/S07.

[15] E. J. Post, "Sagnac effect," *Rev. Modern Phys.*, vol. 39, no. 2, pp. 475–494, Apr. 1967, doi: 10.1103/RevModPhys.39.475.

[16] S. R. Sandoghchi et al., "Optical side scattering radiometry for high resolution, wide dynamic range longitudinal assessment of optical fibers," *Opt. Exp.*, vol. 23, no. 21, pp. 27960–27974, Oct. 2015, doi: 10.1364/OE.23.027960.

[17] M. J. Li, J. A. West, and K. W. Koch, "Modeling effects of structural distortions on air-core photonic bandgap fibers," *J. Lightw. Technol.*, vol. 25, no. 9, pp. 2463–2468, Sep. 2007, doi: 10.1109/JLT.2007.902744.

[18] E. N. Fokoua, D. J. Richardson, and F. Poletti, "Impact of structural distortions on the performance of hollow-core photonic bandgap fibers," *Opt Exp.*, vol. 22, no. 3, pp. 2735–2744, Feb. 2014, doi: 10.1364/OE.22.002735.

[19] X. B. Xu, X. Yuan, F. Y. Gao, X. Wang, and N. Song, "Investigation of longitudinal uniformity of the core structure in a hollow-core photonic bandgap fiber," *Opt. Exp.*, vol. 29, no. 23, pp. 37534–37540, Nov. 2021, doi: 10.1364/OE.442710.

[20] L. Wang et al., "Thermal sensitivity of birefringence in polarization-maintaining hollow-core photonic bandgap fibers," *Photonics*, vol. 10, no. 2, Jan. 2023, Art. no. 103, doi: 10.3390/photonics10020103.

[21] X. Chen et al., "Highly birefringent hollow-core photonic bandgap fiber," *Opt. Exp.*, vol. 12, no. 16, pp. 3888–3893, Aug. 2004, doi: 10.1364/OPEX.12.003888.

[22] M. N. Petrovich, F. Poletti, A. V. Brakel, and D. J. Richardson, "Robustly single mode hollow core photonic bandgap fiber," in *Proc. Opt. Fiber Commun. Conf.*, San Diego, CA, USA, 2008, Paper OThR4.

[23] N. A. Mortensen and M. D. Nielsen, "Modeling of realistic cladding structures for air-core photonic bandgap fibers," *Opt. Lett.*, vol. 29, no. 4, pp. 349–351, Feb. 2004, doi: 10.1364/OL.29.000349.

[24] R. Amezcua-Correa, N. G. R. Broderick, M. N. Petrovich, F. Poletti, and D. J. Richardson, "Design of 7 and 19 cells core air-guiding photonic crystal fibers for low-loss, wide bandwidth and dispersion controlled operation," *Opt. Exp.*, vol. 15, no. 26, pp. 17577–17586, Dec. 2007, doi: 10.1364/OE.15.017577.

[25] H. B. Cai et al., "Thin-diameter polarization maintaining hollow-core photonic bandgap fiber for fiber optic gyroscope," *Opt. Fiber Technol.*, vol. 55, 2020, Art. no. 102141, doi: 10.1016/j.yofte.2020.102141.

[26] H. K. Kim, M. J. F. Digonnet, and G. S. Kino, "Air-core photonic-bandgap fiber-optic gyroscope," *J. Lightw. Technol.*, vol. 24, no. 8, pp. 3169–3174, Aug. 2006, doi: 10.1109/JLT.2006.880689.